Marine Pollution Bulletin 189 (2023) 114823

Contents lists available at ScienceDirect

Marine Pollution Bulletin

journal homepage: www.elsevier.com/locate/marpolbul

Stimulation of oxalate root exudate in arsenic speciation and fluctuation with phosphate and iron in anoxic mangrove sediment

Kang Mei [a,b], Jingchun Liu [a,*], Liyang Xue [a], Jicong Xu [b], Wanlin Jiang [a], Zhiwen Tan [a], Anran Li [a], Jinyi Qu [a], Chongling Yan [a,b]

[a] Key Laboratory of Ministry of Education for Coastal and Wetland Ecosystems, Xiamen University, Xiamen 361102, China
[b] State Key Laboratory of Marine Environmental Science, Xiamen University, Xiamen 361102, China

ARTICLE INFO

Keywords:
Oxalate ligand exchange
Reduced dissolution
Rhizospheric interactions
Mutual transformations
Competitive adsorption

ABSTRACT

Mutual transformations of rhizospheric arsenic (As) in pollution-prone mangrove sediments affected by root exudate oxalate were simulated. This study focuses on the effect of oxalate on As release, mobilization, and phase speciation associated with P and Fe was examined under anoxic conditions in time-dependent changes. Results showed that oxalate addition significantly facilitated As–Fe–P release from As-contaminated mangrove sediments. Sediment As formed the adsorptive and the carbonate-binding fractionations, facilitating the re-adsorption processes. Solution As and As^{5+} correlated with NaOH–P positively but with $NaHCO_3$–P and HCl–P negatively. Dominant Fe^{3+} (>84 %) from the amorphous Fe regulated suspension changes and then time-dependent co-precipitation with As and P. Sediment P formed strong complexes with Fe oxides and could be substituted for As via STEM analysis. Oxalate ligand exchange, competitive adsorption of oxalate, and Fe-reduced dissolution are confirmed to involve, allowing for an insight As/P/Fe mobilization and fate in mangrove wetland.

1. Introduction

Arsenic (As) is a metalloid characterised by non-degradation, strong mobility and persistent toxicity, which induce adverse changes in coastal wetlands (Li et al., 2017a). The bioavailability and toxicity (As^{3+} > As^{5+} > MMA/DMA) of As vary in global natural environments (Huang et al., 2012; Mandal and Suzuki, 2002). Sediment collected from Futian mangroves, Shenzhen, China, has an As content of up to 200 mg kg^{-1}, which indicates a high risk of As pollution (Li et al., 2017b). Industrial and domestic effluent discharges result in As levels of up to 111 mg kg^{-1} in mangrove sediments in Baja California peninsula, Mexico (Leal-Acosta et al., 2010). In addition, As enrichment has been observed in mangrove sediments in Brazil, India and other mangrove ecosystems (Mandal et al., 2019; Mirlean et al., 2012; Nguyen et al., 2019). The distribution, migration and speciation of As in wetlands are influenced by various factors, such as oxidation potential (Eh), pH, mineral oxides, sulphides, organic matter content, plants, and microorganisms (Jian et al., 2019; Luo et al., 2020; Mei et al., 2020; Mei et al., 2022). Eh was found to be a critical factor controlling the dynamics of compounds (DOC and sulphides) and arsenic species (organic and inorganic) in the floodplain, freshwater marsh, or coastal soil since oxidation processes prevail at high Eh whereas reduction processes dominate at low Eh (Frohne et al., 2011; LeMonte et al., 2017; Shaheen et al., 2016). In the redox chemistry of S, metal immobilization can be induced under anoxic conditions due to the presence of hardly soluble sulphides, but the release of As may be attributed to dissolution of sulphides under oxidizing conditions (Frohne et al., 2011; LeMonte et al., 2017; Shaheen et al., 2016).

The root system is the main pathway to secret exudates and oxygen to the rhizosphere, but also uptake and translocate As from sediments to its aerial plant parts. Root−sediment interactions and rhizospheric behaviours (e.g. adsorption, fixation, phytoextraction, and secretion) are accessible perspectives for elucidating As accumulation in plants, which can be applied for As pollution phytoremediation. Low-molecular-weight organic acids (LMWOAs) in the rhizosphere secreted by roots were often associated with exposure to pollutants such as heavy metals Cd, Cr, and Pb (Chancui et al., 2019; Liu et al., 2007; Lu et al., 2007), metalloid inorganic/organic As (Gasecka et al., 2021; Magdziak et al., 2020; Mei et al., 2021), and organic pollutant polycyclic aromatic hydrocarbons (Jiang et al., 2017). For instance, citric acid, acetic acid, and oxalic acid were the maximum released LMWOAs in the plant root rhizosphere (supplementary Table S1). LMWOAs constitute up to 10 %

* Corresponding author.
E-mail address: liujingchun@xmu.edu.cn (J. Liu).

https://doi.org/10.1016/j.marpolbul.2023.114823
Received 24 September 2022; Received in revised form 4 March 2023; Accepted 6 March 2023
Available online 15 March 2023

of DOC in rhizospheric soil solution, and the concentration of LMWOAs range from a micromole (0.1 μmol L^{-1}) to millimole (10 mmol L^{-1}) (Geng et al., 2020; Jones et al., 2005; Strobel, 2001; Xiang et al., 2020). In our previous study, the rhizospheric exudation of LMWOAs from mangrove seedlings was examined to understand As phytoextraction, removal and detoxification in wetland sediments. Results showed that the roots of *Avicennia marina* seedlings secreted the maximum amounts (56.9 %–82.1 %) of oxalic acid, a LMWOA, in response to inorganic arsenite (As^{3+}) exposure (Mei et al., 2021). Oxalate consists of two carboxyl functional groups and is a commonly occurring substance secreted by plant roots and vegetables, which can effectively inhibit contaminant sorption to soils by decreasing hydrophobic force, electrostatic attraction, ligand exchange, and cation-bridge effect (Jones et al., 2003; Xiang et al., 2020). Oxalate was also reported as a valuable exudate for metal remediation due to its high chelating capacity with heavy metals (Kim and Baek, 2015). The extraction of As by oxalate significantly enhanced the release of As from As-loaded ferrihydrite at the pH range of 4 to 8 (Mohapatra et al., 2005). Therefore, oxalate, with low toxicity characteristic and a limited effect on sediment microenvironment, has been used to investigate the significance of effectively remediating As-contaminated sediments.

Iron (Fe) and phosphorus (P) also play important roles in sediment environments; the adsorption−desorption capacity and co-precipitation of Fe and P may control As migration and transformation in wetlands. For instance, the main mineral adsorbents of Fe oxide/hydroxide fractionations (e. g. amorphous and crystalline Fe) in soils exhibit a strong binding capacity to As (Manning et al., 1998). Amorphous Fe has more binding reaction sites due to its large surface (compared with crystalline Fe), which can increase adsorption with As (Bowell, 1994). Moreover, Fe content and speciation, such as reduced dissolution in sediments, affect As migration and transformation (Mei et al., 2020). In addition, the Fe−P coupling mechanism deemed that phosphate release and conversion were largely controlled by reductive dissolution of Fe oxides (Rozan et al., 2002; Sun et al., 2016). The overlying water of the Jiulong River Estuary contains excessive dissolved P (0.05–1.5 mg L^{-1}), which may induce pollution via P accumulation (Pan et al., 2019). A study on the effect of P levels on the formation of amorphous Fe minerals demonstrated that P release is mainly related to amorphous Fe and aluminium (Al) oxides, and the adsorption of some anions (e. g. PO3–4) inhibits the Fe oxides/hydroxides generated from amorphous forms to crystalline forms (Ji et al., 2019). In the rhizosphere, dissolved P associated with the mineral composition of the Fe oxides on root surfaces forms Fe/Mn plaque, which determines the phytoextraction and accumulation of metal(loid)s by mangrove plants (Dai et al., 2017). Fe plaque formation on the root surfaces of wetland rice (*Oryza sativa* L.) was also promoted by low-P conditions, thereby enhancing As transport from the sediment to the aerial plant parts (Hu et al., 2005). Since P and As have similar chemical characteristics (belong to the same family in the periodic table), As could be substituted for deficient P in biogeochemical processes (Ghosh et al., 2015). For instance, PO3–4 and AsO3–4 have strong affinities with the surfaces of Fe minerals, which depend on the complexing ability (mainly through ligand exchange reactions for binding to surface groups) and particulate attraction or electrostatic interaction with surface-charged oxides/hydroxides (Stumm, 1992). Elevated levels of dissolved P (0.2 mg L^{-1}) can compete with As for the adsorption sites on sediment surfaces and accordingly increase As mobilization, leading to conversion of the adsorbed As to the dissolved As (Jiao et al., 2012; Pan et al., 2019; Sun et al., 2017). In addition to the competitive adsorption of phosphate, As^{3+} and As^{5+} are generated when P is added to As-enriched sediments, which can be attributed to colloidal aggregation. Phosphate can promote the release of As by displacing anions, participating in complexation reactions or occupying oxide adsorption sites (Esteban et al., 2003). In summary, Fe oxides/hydroxides are key factors in controlling the release of P and As, and P and Fe jointly affect the migration and transformation of As at sedimentary interfaces.

Degradable oxalate is a common root-secreted LMWOA and is a ubiquitous occurrence in mangrove rhizospheres (Jian et al., 2019; Jiang et al., 2017; Lu et al., 2007; Mei et al., 2021). As far as we known, root rhizospheric microenvironment especially root-soil interfaces are lack of on-site detailed research due to the flooding or submerge of mangrove root system in the wetland. In this work, the dynamics of the belowground rhizospheric interfaces of mangroves were simulated under the influence of oxalate to elucidate As migration behavior and speciation changes. Fe plays the key role in sedimentary environments, and oxalate is occurring to affect As release (Kim and Baek, 2015). Therefore, The effect of oxalate on As release, mobilization and phase fractionation in interactions with P and Fe in anaerobic wetland sediments was explored to reveal the underlying mechanisms that may be involved in rhizospheric processes. This study aims to understand the potential mechanism of As release extracted by oxalate from As-enriched mangrove sediments combined with P and Fe to supplement the existing knowledge on As-remediated metal(loid)-contaminated wetlands.

2. Materials and methods

2.1. Sampling and characteristics

The natural mangrove sediments were obtained from Zhangjiangkou Mangrove Forestry National Nature Reserve in Fujian Province, China (24° 24′ N, 117° 55′ E) that is showed in Fig. S1. The total As in the sediment was 17.38 ± 0.72 mg kg^{-1} in dry weight (Table S2), which is very close the Grade I threshold (20 mg kg^{-1}, pH > 7.5) for agricultural land of Environmental Quality Standards for Soils, China (GB15618–2008). The sediments were prepared and stored in accordance with the previous procedure for later use (Mei et al., 2020). To sum up, the sediments were mixed and homogenised with extra inorganic trivalent arsenite solution ($NaAsO_2$) up to 0 mg kg^{-1} As (As0; control group), 40 mg kg^{-1} As (As40, Double background value and close to threshold of non-agricultural land) and 60 mg kg^{-1} As (As60, Triple background value and close to threshold of industrial land) in dry weight, not including background value. The characteristics of the natural sediment background values are shown in the Table S2. The national criteria reference material (CRM) of stream sediment (GBW07318, China) was checked for procedural accuracy.

2.2. Sediment elemental speciation and release

The mechanisms of oxalate–enhanced As release from mangrove As-enriched sediment were explored by a series of batch experiments in an anoxic N_2–blowing box. To investigate the effect of effective exchangeable ligands and competitive adsorption on As speciation in mangrove sediments, the three gradient concentrations of oxalate solution (0, 3 and 5 mmol L^{-1}, soil solutions are commonly in the range 0.1–10 mmol L^{-1}) were added into the As-enriched sediment (As0, As40, and As60). To observe the influence of oxalate reaction time on As release into the aqueous phase, the sediment-oxalate mixtures were incubated with a fixed oxalate concentration (3 mmol L^{-1}) for the different reaction times of 6 h, 2 d, and 8 d. The batch experiment in triplicate was conducted at 25 °C in a 50–mL polyethylene centrifuge tube containing 30–mL suspension of oxalate solution (N_2–blowing for 30 min) and 1–gram of sediment. The centrifuge tube was oscillated via a vortex (MX-S, Scilogex, USA) and incubated for 24 h in a shaker at 25 °C and a rate of 200 rpm (Saifu BHWY-200 Shaker, China). After incubation, the supernatant was filtered (0.45-μm, Membrana Germany) immediately after centrifugation at the rate of 8000 rpm for 10 min. The sediments in the tube were collected and stored at −20 °C for subsequent analysis.

2.3. Reaction time-dependent isotherm dynamics

The estimation of the dynamic equilibrium was investigated for comprehending adsorption isotherm on As release and variations in

solution. A dose of 3 mmol L^{-1} was applied into the As40 enriched sediments to observe temporal responses based on the results of the previous experiment. The reactor tubes were incubated in the rotary shaker at 200 rpm and 25 °C in the dark for 6 h and 12 h and 1, 2, 4, 7 and 14 days. The centrifuged supernatant (8000 rpm for 10 min) was further passed through a 0.45-μm filter before analysis. Triplicated samples were collected to determine As/P/Fe fractionations variations in the sediment and supernatant as well as the pH.

2.4. Phosphate competitive adsorption and solid phase characterization

Subsamples (~1 g) of the high As-loaded sediments (60 mg kg^{-1}) were weighed, freeze-dried (−50 °C), ground, and sieved (2-mm) for observing the competitive adsorption of phosphate on As release. Specifically, based on the elemental P fractionation in mangrove sediment (total in 250–300 mg kg^{-1}), different gradient concentrations of phosphate solution (0, 10, 25, 40, 50, 60, 80, and 100 mg L^{-1} KH_2PO_4, pH = 6.85 CPBS), and four phosphate concentrations (P0, P25, P50, and P100) with the setting pH level (3, 5, 7, 9 and 11) were added to the As-enriched sediments under the anoxic conditions. The separation of the solid and liquid phases was conducted after incubation and centrifugation, and supernatant As variations was determined using the method mentioned before. The energy spectrum and element composition of freeze-dried sediments were analyzed to present the newly formed elemental distribution.

The adsorption capacity of As-enriched sediments to P was assessed using two isothermal adsorption models of Freundlich and Langmuir (Adamson and WJJOTES, 1960). Langmuir nonlinear model is monolayer adsorption with the maximum adsorption surface (Weber and Chakravorti, 1974),which for illustrating the monolayer adsorption process as described in the following Equations (Wu et al., 2020):

$$Q_e = Q_0 \times \frac{K_L C_e}{1 + K_L C_e} \tag{1}$$

Furthermore, Freundlich model is used for non-uniform adsorption sites, where existing exchangeable multilayer adsorption-desorption processes.

$$Q_e = K_F \times C_e^{1/n} \tag{2}$$

$$logQ_e = \frac{1}{n} logC_e + logK_F \tag{3}$$

The content of adsorption when the solution-sediment reached adsorption equilibrium.

$$Q_e = \frac{V(C_0 - C_e)}{M} \tag{4}$$

The adsorption efficiency (η %) of the sediment against P.

$$\eta = \frac{(C_0 - C_e)}{C_0} \times 100\% \tag{5}$$

Where Q_0 (mg kg^{-1}) is the maximum saturated adsorption capacity of P in theory; and Q_e is the equilibrium absorption capacity; K_F is the P adsorption coefficient; C_e is the P concentration in the solution at equilibrium condition (mg L^{-1}); K_L represents the binding energy , when $K_L > 1$ indicates that the adsorption capacity is pretty strong; The index $\frac{1}{n}$ is the measure constant of sorption intensity, and $\frac{1}{n} < 1$ indicates that sorption capacity is only slightly suppressed at lower equilibrium concentration (Hasany et al., 2002).

2.5. Analysis

The analysis of total organic matter of sediments was applied with weight combustion subtraction (460 °C for 6 h) method in a muffle furnace. The C, H, and N was analyzed with an element analyser (Elementar Analyse Systeme GmbH, Hanau, Germany). The extracted procedures of As, P, and Fe fractionation in sediments were listed in **Table S3**. The sequential extraction procedures, including five phases of As fractionations: ① adsorbed As; ②carbonate–binding As; ③ amorphous Fe–binding As; ④ crystalline Fe–binding As; and ⑤ residual As were fully described in the previous studies (Luo et al., 2020; Xu et al., 2016). The analysis of As fractionations in the filtrate after extraction of was performed on atomic fluorescence spectrometry (AFS-930, Beijing Jitian Co. Ltd., China). A sequential available P fractionation was divided into four fractions as the following (i) $NaHCO_3$ extractable P ($NaHCO_3$-P), (ii) NaOH extractable P (NaOH-P), and (iii) HCl extractable P (HCl-P) (Hedley et al., 1982; Linquist et al., 2011), the rest was regarded as the residual part (Residual-P). The detection of P in the filtrate is by using ammonium molybdate UV–vis spectrophotometry (Beijing Ruili Co. Ltd., China). The amorphous Fe (reactive and poorly crystalline Fe) and crystalline Fe in the solid phase were extracted by ammonium oxalate buffer (0.2 mol L^{-1} NH_4-oxalate/oxalic acid, pH 3.25, 20 h) and DCB solution (sodium dithionite 50 g L^{-1} in 0.2 mol L^{-1} sodium citrate/0.35 mol L^{-1} acetic acid, pH 4.8 Buffer; 2 h) in the dark, respectively (Burton et al., 2007; Jian et al., 2017; Kostka and Iii, 1994). The extractable Fe was measured using atomic absorption spectroscopy (AAS vario 6, Thermo Fisher).

For aqueous phase, the pH of the supernatant and sediment (sediment: water = 1: 2.5) was measured using a pH meter (Leici PHS-2F, Shanghai, China). The concentration of Fe^{2+} in the supernatant was measured using 1,10-phenanthroline spectrophotometry at 510 nm via a UV–vis spectrophotometer (Beijing Ruili Co. Ltd., China). The Fe in the filtrate (including the extracted amorphous and crystalline Fe) was reduced to Fe^{2+} with hydroxylamine hydrochloride ($NH_2OH{\cdot}HCl$) and sulphuric acid. The Fe^{3+} was calculated by subtracting the Fe^{2+} from the total Fe. The amounts of inorganic As^{3+} and As^{5+} in the supernatant was separated and detected using HPLC-HG-AFS (Tanta technologies, Gunt, Germany) as our previous described method (Mei et al., 2022). The ultrastructure image and element composition characteristics of freeze-dried sediments after incubation were evaluated via STEM-EDAX (FEI Quanta 650 FEG, America). We used the standard addition method for the assessment of inorganic arsenic due to the lack of criteria reference materials. The supernatants were filtered (0.45 μm) and stored at −20 °C after centrifugation (8000 rpm for 5 min) until analysis. Recovery levels (85 %–115 %) were acceptable for all the elements determined. All chemical reagents applied in the present study were of chromatographic grade.

3. Results and discussion

3.1. Enhanced sediment elemental fractionation and release

The fractionations of certain elements extracted using the common root exudate oxalate from As-contaminated sediments were estimated with the addition of various concentrations of oxalate. The fractions of As, P and Fe from the sediments are summarised in Fig. 1. At the fixed level of 3 mmol L^{-1} oxalate, the greater the As content of the sediment, the better the detection of the adsorbed As (As_{ad}) and the residual As (As_{res}). The maximum concentration of carbonate- and Mn-binding As (As_{cab}) formed in the As60 treatment (Fig. 1A). Less sediment As fractions were found along with the increment oxalate due to As mobilization to the upper solution phase. The fractions of all three P fractionations increased with the As level but decreased with the oxalate concentration (Fig. 1C and D). There was no significant difference ($p > 0.05$) between the As-enriched treatment groups for both amorphous and crystalline Fe (Fig. 1E). Crystalline Fe increased with the oxalate concentration, whereas amorphous Fe showed the opposite tendency (Fig. 1F). Similar trends of the As fractions (As_{cry} and As_{amo}) were measured (Fig. 1A and B), demonstrating the reductive dissolution of As associated with Fe oxides (Kim and Baek, 2015). As can be remobilised and released into porewater from the reductive dissolution of Fe—Mn

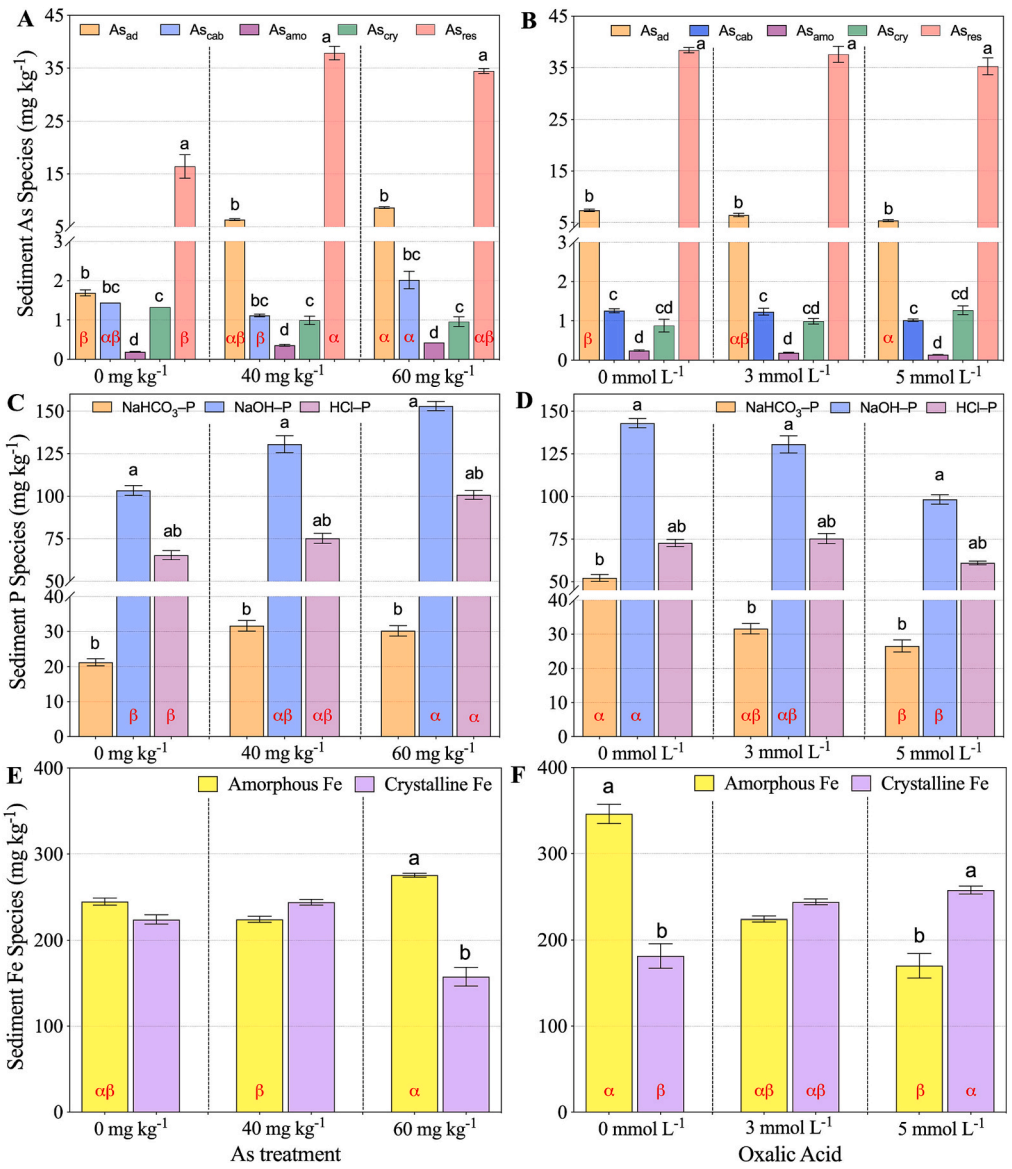

Fig. 1. The fractionation of As, P, and Fe species in the sediment for oxalate extraction from As-enriched mangrove sediments under anoxic incubation. A&B. the five As species in the post-extraction sediments including: ① the adsorption species of As (As_{ad}), ② the carbonate binding species of As (As_{cab}), ③ the amorphous iron binding species of As (As_{amo}), ④ the crystalline iron binding species of As (As_{cry}), ⑤ the residue As species (As_{res}); C&D. the three P species in the post-extraction sediments including: I). the exchangeable species of P ($NaHCO_3$-P), II). the amorphous and crystalline Fe and Al binding species P (NaOH-P); III). the calcium-binding species of P (HCl-P); E&F. the amorphous and the crystalline Fe species. All data were calculated as the relative concentrations to dry sediment weight (mg kg^{-1} DW), Mean ± SE, $n = 3$. Different letters in each treatment indicate significant differences at the level of $p < 0.05$. English lowercases (a, b, and c, etc.) for all the determined As fractions under the same treatment of As addition or oxalate concentration, while Greek lowercases (α and β, χ, and δ) for the same As fraction with the same color bar determined in increasing As addition groups (As0, As40, and As60) or increasing oxalate extraction (0, 3, and 5 mmol L^{-1}) treatments separately.

oxides and/or reduction of the adsorbed As^{5+} to As^{3+} under anoxic conditions, with weaker affinity levels for minerals (Bose and Sharma, 2002).

The variations in the solution were estimated after oxalate interacted with the sediments for different reaction durations. The dissolved As, P and Fe fractionations/species (total Fe, Fe^{2+} and Fe^{3+}) in the aqueous supernatant during the three incubation periods are presented in Fig. 2. The results on the oxalate-extractable As showed a gradually increasing trend along with As level and oxalate concentration. The solution As reached the maximum concentration at 6 h (0.44 mg L^{-1}) and then decreased at 2 and 8 days under the same level of As contamination or oxalate addition. Similar results were observed for the solution P, which exhibited the highest value of 0.20 mg L^{-1} but showed an obvious drop of 0.01–0.04 mg L^{-1} at 2 days (Fig. 2B). The solution pH in all treatments clearly decreased along with the oxalate concentration but slightly increased with the incubation time. The presence of As-enriched contents had a limited influence on the pH change (Fig. 2C).

The concentrations of Fe^{2+}, Fe^{3+} and Fe in response to oxalate in the filtrates are shown in Fig. 2. All the Fe fractionations were significantly ($p < 0.01$) enhanced by the addition of oxalate in comparison with the control group. In the absence of oxalate, the average efficiencies of extracting Fe^{2+}, Fe^{3+} and total Fe using ultrapure water were <16.6 %, 5.87 % and 6.58 %, respectively. Oxalate ($C_2O_4^{2-}$) is a mild reducing agent ($E^\circ = -0.18$) but a strong chelating agent; it can form strong complexes with Fe^{2+} and Fe^{3+} (Kim and Baek, 2015). Carboxyl group ($C_2O_4^{2-}$) could replace two OH^- on the iron hydroxide surface and electron transferred from $C_2O_4^{2-}$ to Fe^{3+}, resulting in mineral structure collapse to release Fe^{2+} and As into the solution (Onireti and Lin, 2016). Reductive Fe^{2+} was also found to be a major species of the 2 mmol L^{-1} oxalate treatment in our previous study (Mei et al., 2021). In the present work, the higher oxalate concentrations (3 and 5 mmol L^{-1}) were associated with greater release of Fe^{3+} (84.6 %–91.1 %) and total Fe (74.9–135.3 mg L^{-1}) into the aqueous phase. Soluble Fe^{3+} oxalates [$Fe(C_2O_4)_2]^-$ and oxalate complexes were probably formed under a sufficient amount of oxalate (Onireti and Lin, 2016). Humboldtine ($Fe(C_2O_4)\cdot 2H_2O$), an Fe oxalate phase, has also been observed when 10 mmol L^{-1} oxalate was added to dithionite (Kim and Baek, 2015).

3.2. Dynamics of elemental release and reduction

The solution As decreased from its peak value of 122 μg L^{-1} (6 h) to about 6 μg L^{-1} (12 d) as the reaction time increased (Fig. 3A). The Fe content for oxalate application significantly increased in the first stage

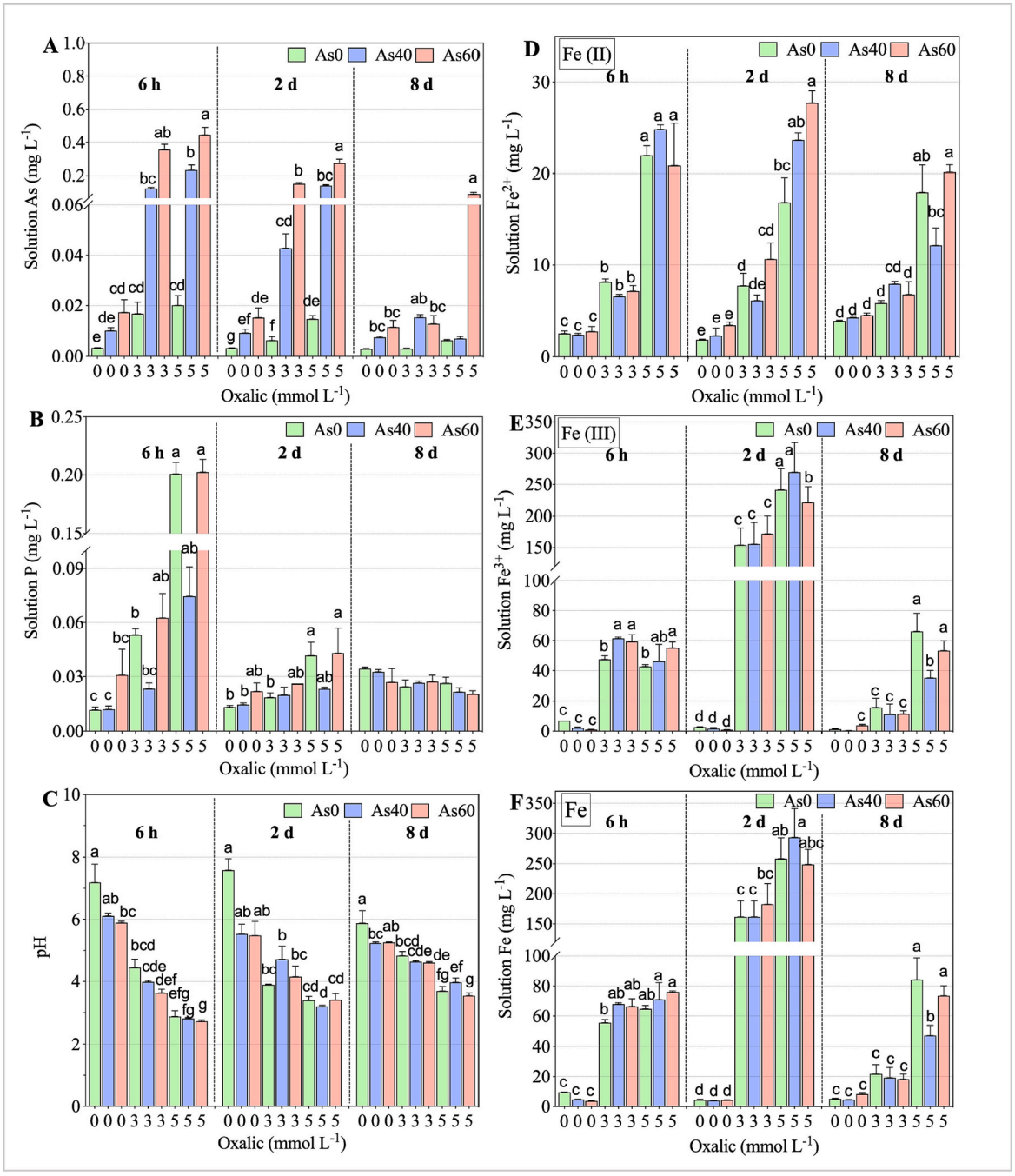

Fig. 2. The variations in the supernatant of oxalate extracts for concentrations treatment (0, 3, and 5 mmol L^{-1}) and reaction time incubation treatment (6 h, 2 d, and 8 d) for the As-enriched sediments (0, 40, and 60 mg kg^{-1}). A. the total As concentration in the solution; B. the total P in the solution; C. variations of the solution pH; D. the ferrous iron (Fe^{2+}) in the solution; E. the ferric iron (Fe^{3+}) in the solution; and F. the total iron (Fe) in the solution; All parameters were calculated as the concentrations in oxalate extracts (mg L^{-1}), Mean ± SE, $n = 3$. Ultrapure water extraction was used as the control check. Different letters in each same reaction time treatment indicate significant differences at the level of $p < 0.05$.

(6 h), reached its maximum value at 2 days and then gradually decreased, whereas the solution P content remained stable at 13–25 μg L^{-1}. Organic acid root exudates can enhance metal(loid) mobility that combined with Fe—Mn oxides, which act as stabilising agents in sediments under pH loss and metal complex formation (Vitkova et al., 2015). Furthermore, the increasing pH trend (3.99–5.07) may have been due to the formation of solid hydroxides and proton consumption via mineral dissolution (Mei et al., 2021; Wang and Wang, 2017).

The amorphous and crystalline Fe contents in the solid phase declined during incubation at 4 days compared with the first two stages (6 h and 12 h). The amorphous Fe extraction from the As-enriched sediments showed a similar ascending trend with the sediment P as the reaction time increased from 4 days, indicating an Fe-meditated precipitation of the Fe oxalate phase. However, there was a slight decrease in the extraction of crystalline Fe, and it was highly correlated with the sediment As. A similar study reported that approximately 40 % As is associated with crystalline Fe oxides, whereas no >20 % As is bound to amorphous Fe oxides (Kim and Baek, 2015).

Further analysis of the sediment speciation of As after incubation revealed that As_{res} (60.6 %–88.8 %) and As_{ad} (7.3 %–23 %) accounted for the two largest parts of the total As (Fig. 4). The significant ascending trend ($p < 0.01$) of As_{ad} in response to the reaction time suggested that

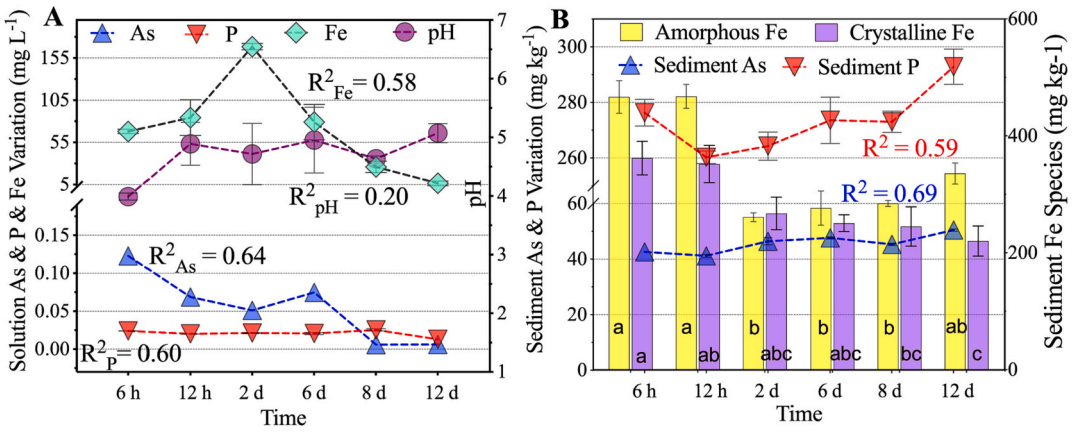

Fig. 3. The assessment of As adsorption–desorption associated with Fe and P in the oxalate solution–sediment mixture after different incubated reaction time. A for the variations of As, P, Fe and pH in the solutions. B for the changes of the total As, Fe species, and the total P in the sediments. All data were calculated as the relative concentrations to oxalate extracts (mg L^{-1}) or dry sediment weight (mg kg^{-1} DW), Mean ± SE, n = 3. Different lowercases (a, b, and c, etc.) in each determined Fe species fraction with the same color bar indicate significant differences at the level of $p < 0.05$.

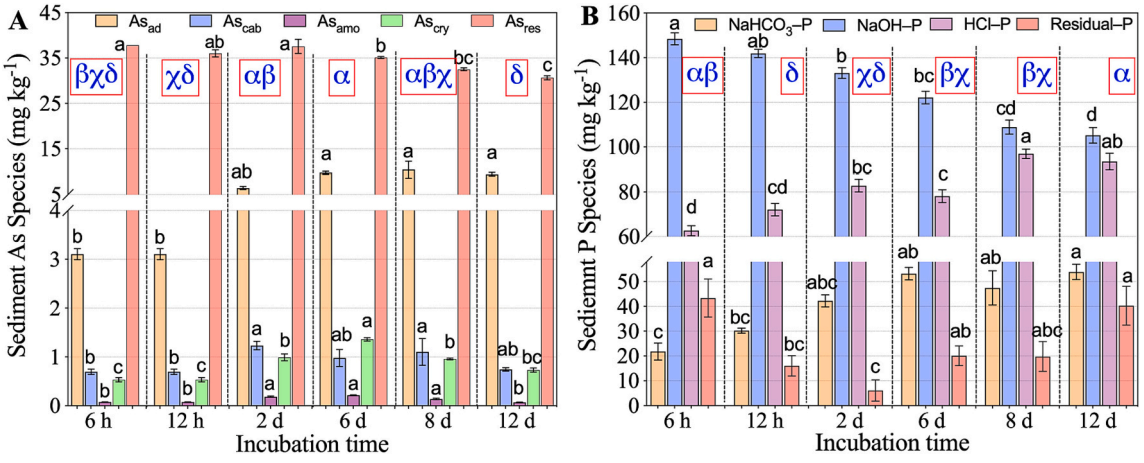

Fig. 4. The five determined As species and the four P species in the sediment after different incubated reaction time. All data were calculated as values extracted from dry sediments (mg kg^{-1} DW). A. the five As species fractions in the post-extraction sediments including: ① the adsorption species of As (As_{ad}), ② the carbonate binding species of As (As_{cab}), ③ the amorphous iron binding species of As (As_{amo}), ④ the crystalline iron binding species of As (As_{cry}), ⑤ the residue As species (As_{res}); B. the three P species in the post-extraction sediments including: (i) the exchangeable species of P ($NaHCO_3$-P), (ii) the amorphous and crystalline Fe and Al binding species P (NaOH-P), and (iii) the calcium-binding species of P (HCl-P). Different English lowercases (a, b, and c, etc.) in each determined fraction with the same color bar indicate significant differences at the level of $p < 0.05$, while Greek lowercases in red box (α and β, χ, and δ) represent significant differences for the sum of all determined fractions during incubation. (For interpretation of the references to color in this figure legend, the reader is referred to the web version of this article.)

the readsorption processes of As migrated from the aqueous phase to the solid phase. Similar trends emerged in the results for As_{cab} (0.99–1.23 mg kg^{-1}), As_{amo} (0.14–0.21 mg kg^{-1}) and As_{cry} (0.96–1.36 mg kg^{-1}), which were positively correlated with the total solution As (Fig. 5). However, As_{ad} (6.45–10.4 mg kg^{-1}) and the three above mentioned As fractionations all reached the maximum plateau at 2–8 days (not significant, Fig. 4A), indicating that the sediment may have exceeded its maximum adsorption capacity could be due to pH changes and co-precipitaion (amorphous Fe). The release of As was mainly attributed to the reductive dissolution of amorphous Fe; then the decreased readsorption As could be co-precipitated with the newly formed crystalline Fe minerals (Luo et al., 2020). Meanwhile, the adsorption of As can be strongly impacted by S cycling in reduced soils and Fe is also expected to precipitate as sulphides (Frohne et al., 2011; LeMonte et al., 2017). In this case, reductive dissolution of As-bearing iron compounds induced by oxalate had been reported to facilitate mobilizing As, involved proton attack on As containing iron compounds and organic ligand complexation (Onireti and Lin, 2016). The P fractionation detected versus the reaction time increased from 6 h to 12 days. The $NaHCO_3$–P and HCl–P concentrations at 6 h gradually increased from 21.8 to 53.2 mg kg^{-1} and from 62.6 to 96.9 mg kg^{-1}, respectively; whereas that of the major NaOH–P decreased from 148.5 to 105.2 mg kg^{-1}. The correlation analysis revealed that the solution As was significantly positively correlated with NaOH–P ($R^2 = 0.88$) but negatively correlated with both $NaHCO_3$–P ($R^2 = -0.72$) and HCl–P ($R^2 = -0.95$, Fig. 5).

3.3. As kinetics affected by phosphate and pH

The release of sediment As is highly associated with the P behavior from labile fractions due to their similarity in chemical properties, such as competitive adsorption (Im et al., 2015). The dissimilar extraction efficiencies of released As and inorganic As species (As^{3+} and As^{5+}) were observed against the added phosphate concentration and pH (Fig. 6). The proportion of As^{3+} to the solution As reduced from 22 % to 1.6 % with the increment of added phosphate concentration, maintaining significantly low concentrations of 2.19–5.59 μg L^{-1}. Meanwhile, the

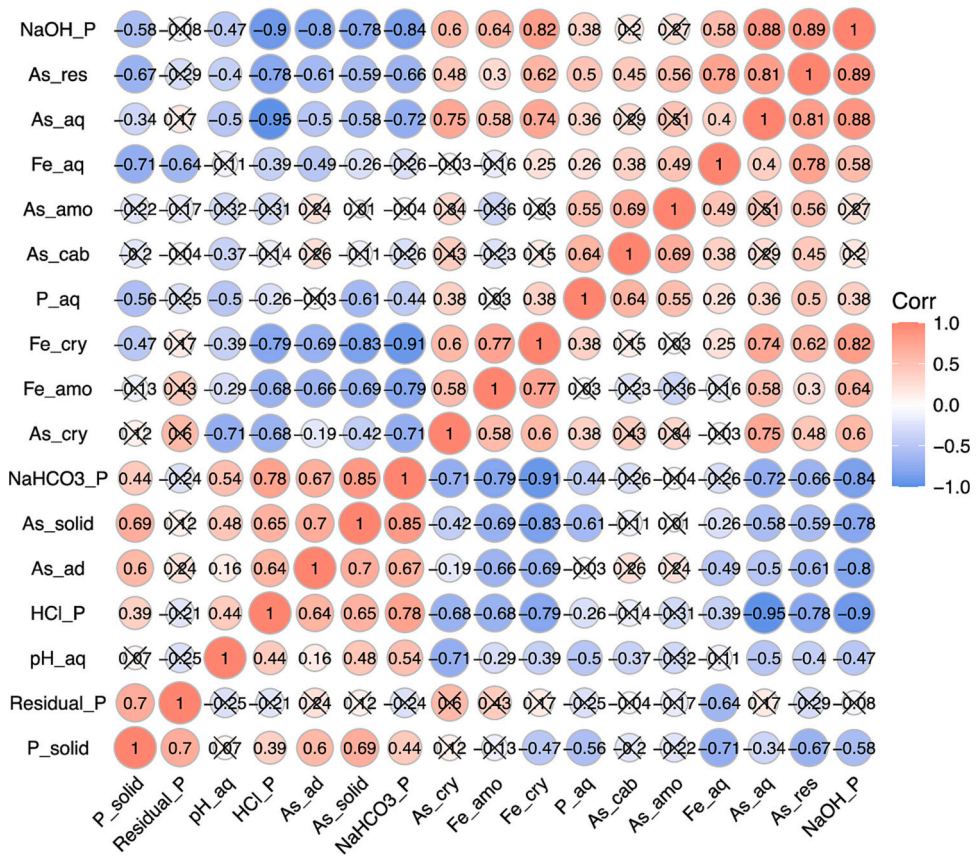

Fig. 5. The correlation of the determined parameters in the supernatant and sediment during oxalate incubation in response to reaction time (n = 18). The insignificant correlation at 0.01 levels are marked in cross signs (two–tailed). Solution As = As_aq, Solution P = P_aq, Solution Fe = Fe_aq, Solution pH = pH_aq, Amorphous Fe = Fe_amo, Crystalline Fe = Fe_cry, Solid As = As_solid, and Solid P = P_solid.

total As and As^{5+} in the solution gradually increased with the phosphate concentration, revealing that PO3–4 ions outcompeted the extracted As present as AsO3–4 for adsorption sites on the Fe oxides (Im et al., 2015; Jain and Loeppert, 2000). Similarly, the Fe concentration in oxalate solution exhibited an increasing trend and then decreased at the addition of 60 mg L^{-1} phosphate (Fig. S2). PO3–4 and AsO3–4 ions can compete for the adsorption sites on the surfaces of Fe—Mn oxides/hydroxides, especially amorphous Fe oxides, forming insoluble compounds with Fe and Al in sediments (Biswas et al., 2018). The total As was highly correlated with P (R^2 = 0.72) and Fe (R^2 = 0.65, Fig. S3), indicating the fate of As is closely related to the redox cycling of Fe and P. As^{5+} occupied a major fraction (48.7 %–91.3 %) of the solution, which may partially be due to the As^{5+} release from the sediments. In addition, the co-existence of Fe^{3+}–Fe^{2+} can promote the oxidation of As^{3+} (Amstaetter et al., 2010). For instance, the Fe^{3+} oxyhydroxides coating a pyrite surface probably led to As^{3+} oxidation in a past study (Zhang et al., 2017), thus maintaining low As^{3+} concentrations (Fig. 6A). The chemical characteristics of Fe plaque adsorbed to the root surface, analyzed via X-ray absorption near-edge structure, show that As and Fe form binuclear ligand complexes, and Fe oxides/hydroxides have a higher affinity for As^{5+} than As^{3+} (Elkhatib et al., 1984; La Force et al., 2000; Manceau et al., 1996; Mohan and Charles, 2007).

The variations of the phosphate concentrations on the As released from mangrove sediments were explored in the presence of PO3–4under various pH-modulated conditions (pH 3, 5, 7, 9 and 11), as shown in Fig. 6B. In the absence of phosphate, As was hardly mobilised from the sediments, regardless of pH change. The efficiency of As extraction was significantly enhanced by the concentration of added phosphate and the increased pH levels. The more the As released from the sediment pool, the higher the occurrence of PO3–4 or the higher the value of the pH except pH 11, where the maximum value of As was observed for P50 addition. These results may indicate that more absorbed PO3–4 and AsO3–4were released form solid phase under alkaline conditions (pH 9 and 11); meanwhile, PO3–4 could probably replace more AsO3–4 and other oxides released into the liquid phase (Im et al., 2015). The increased supply of H^+ at the lower pH also facilitated the adsorption of As by Fe oxides/hydroxides and reduced the mobility of As (Jain et al., 1999).

The adsorption–desorption dynamics of the P in the phosphate–sediment mixtures were assessed by considering isotherm-predicted models of Freundlich's and Langmuir's equations. Results showed that the adsorption efficiency (η = 94.5 %–99 %) of P gradually decreased along with the increase of added phosphate concentration (Fig. 6C). A possible reason is that the surface area of the As-enriched sediment had more adsorption sites at lower P, but high P of similar chemical properties could result in the desorption of retained As thus exhibiting a higher adsorption efficiency (Datta and Sarkar, 2005). The P adsorption efficiency of the sediment was gradually reduced with the increase of P concentration, suggesting that P occupied more adsorption sites, leading to As release (Im et al., 2015). The correlation coefficient values (R^2) of both the Freundlich (R^2 = 0.93) and Langmuir models (R^2 = 0.99) were highly close to unity, indicating that the P adsorption process by As-enriched sediments could be interpreted by both models. The average Q_0 fitted to the Langmuir model was 1825.8 ± 91.6 mg kg^{-1}, and the value of K_L (0.12 ± 0.02) was far <1. Hence, the adsorption binding energy of the As-enriched sediments to P was weak, and it could easily redesorb from the solid phase surface. According to the Freundlich isothermal adsorption model, R^2 = 0.93, and the averages of K_F and n were 352.7 and 0.44, respectively. The n value ($1/n > 1$) indicated that the strong competitive adsorption of P tended to cause As release, which

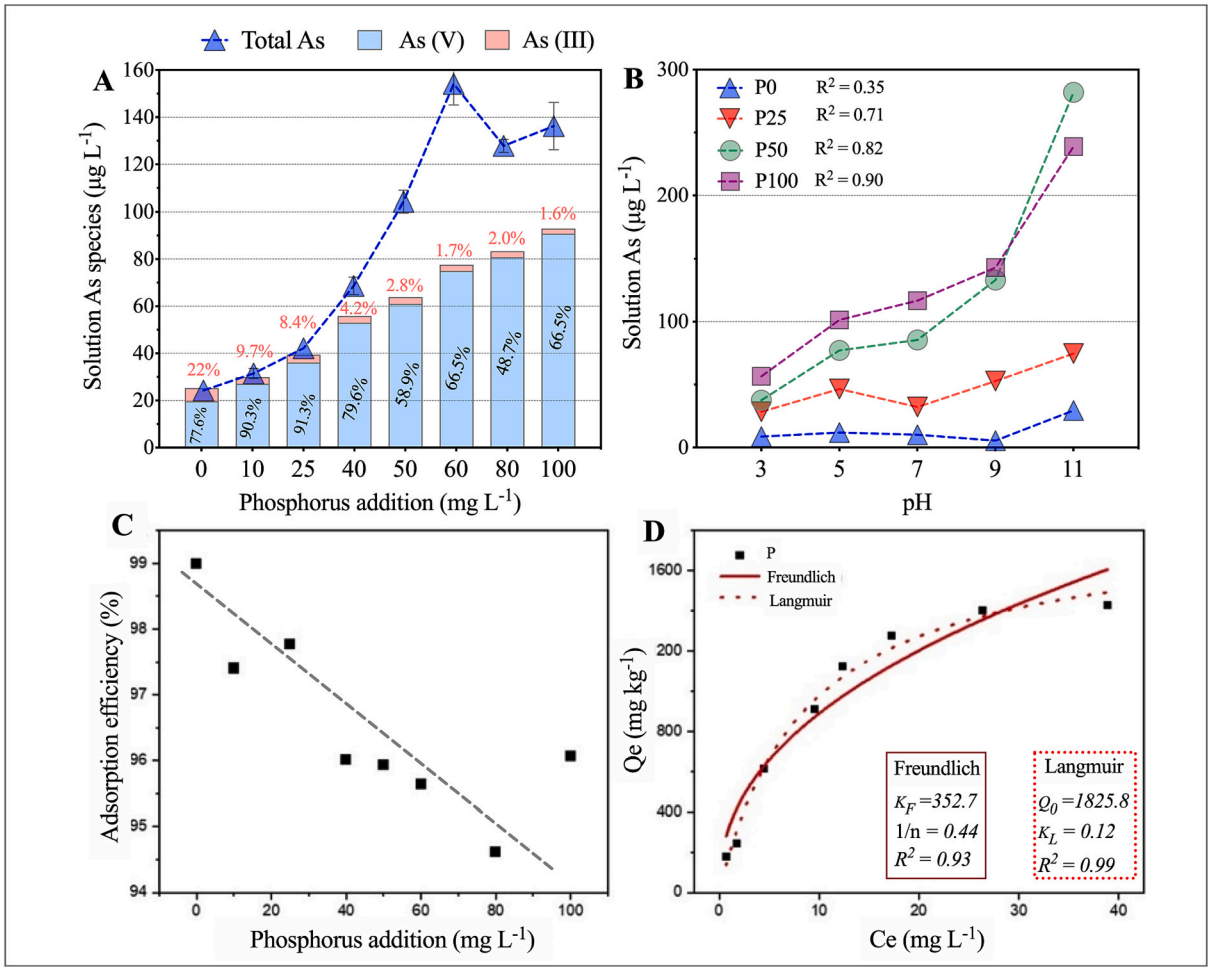

Fig. 6. The variations of As species (μg L^{-1}) and assessment in the extracted solution under P gradients addition and varied pH gradients treatment from the As–enrichment sediments after incubation. A. different P addition treatment, B. the same P level under different pH gradients treatment, C. P adsorption efficiency; and D. the P adsorption isotherm predicted models of Freundlich and Langmuir. Q_0 (mg kg^{-1}) is the maximum saturated adsorption capacity of P in theory; and Q_e is the equilibrium absorption capacity; K_F is the P adsorption coefficient; C_e is the P concentration in the solution at equilibrium condition (mg L^{-1}); K_L represents the binding energy, when $K_L > 1$ indicates that the adsorption capacity is pretty strong; 1/n is the measured constant of sorption intensity and $1/n < 1$ indicates that sorption capacity is only slightly suppressed at lower equilibrium concentration. Mean ± SE, $n = 3$.

was attributed to the presence of added adsorption sites in the sediment. The Langmuir model could better predict the adsorption process, which meant that specific adsorption occurred through a monolayer mechanism. The adsorption efficiency was related to the adsorption sites, and the adsorption process mainly depended on the initial P concentration (Liu and Shen, 2008).

3.4. Sediment ultrastructure and characteristics

The STEM high-resolution image of the freeze-dried sediment samples revealed the surface feature and ultrastructure after the extraction of phosphate addition. The energy spectrum and elemental composition of the mapping data of the freeze-dried As-enriched sediments, obtained via energy-dispersive X-ray analysis, are shown in Fig. 7. Phosphate and arsenate both exhibited a high affinity for mineral surfaces and had a strong adsorption capacity to metal oxides/hydroxides, especially Fe and Al. The elemental distributions of As, P and Fe showed that they combined with each other on the sediment surface. Thus, Fe was a major part of the elemental composition, and the distribution of P was similar to that of As. This also revealed that As and P have the same adsorption sites on the surface of the Fe oxides/hydroxides, demonstrating the existence of competitive adsorption between As and P on the sediment surface. The proportions of P, O and Fe in the sediment significantly increased after P addition (Fig. 7), while that of As did not significantly change, which may be due to the low available content (ppm grade) in the sediments. The affinity of PO3–4and AsO3–4for Fe oxide/hydroxide depended on their complexing capacity through ligand exchange reactions and on their interaction (attraction or electrostatic rejection) with the charge (hydroxyl).

4. Conclusions

Using the combination of phosphate and oxalate, we determined oxalate-mediated As release in time-dependent changes of the total As and selected forms of inorganic As^{3+}, As^{5+} in the solution, and sequentially extracted As speciation fractions in the solid phase associated with Fe (amorphous) and P fractions ($NaHCO_3$–P and HCl–P) under anoxic conditions. High As release was observed in the As-enriched sediments at a wide range of oxalate concentrations, reaction times, added phosphate concentration and pH conditions in a series of incubation experiments. According to observations, the mechanisms involved in the oxalate-promoted release of As were oxalate ligand exchange, the competitive adsorption of oxalate and P and Fe-reduced dissolution/co-precipitation. The findings on the oxalate-enhanced release of As and speciation transformation between dissolved and solid phases supplement the knowledge on As-remediated contaminated

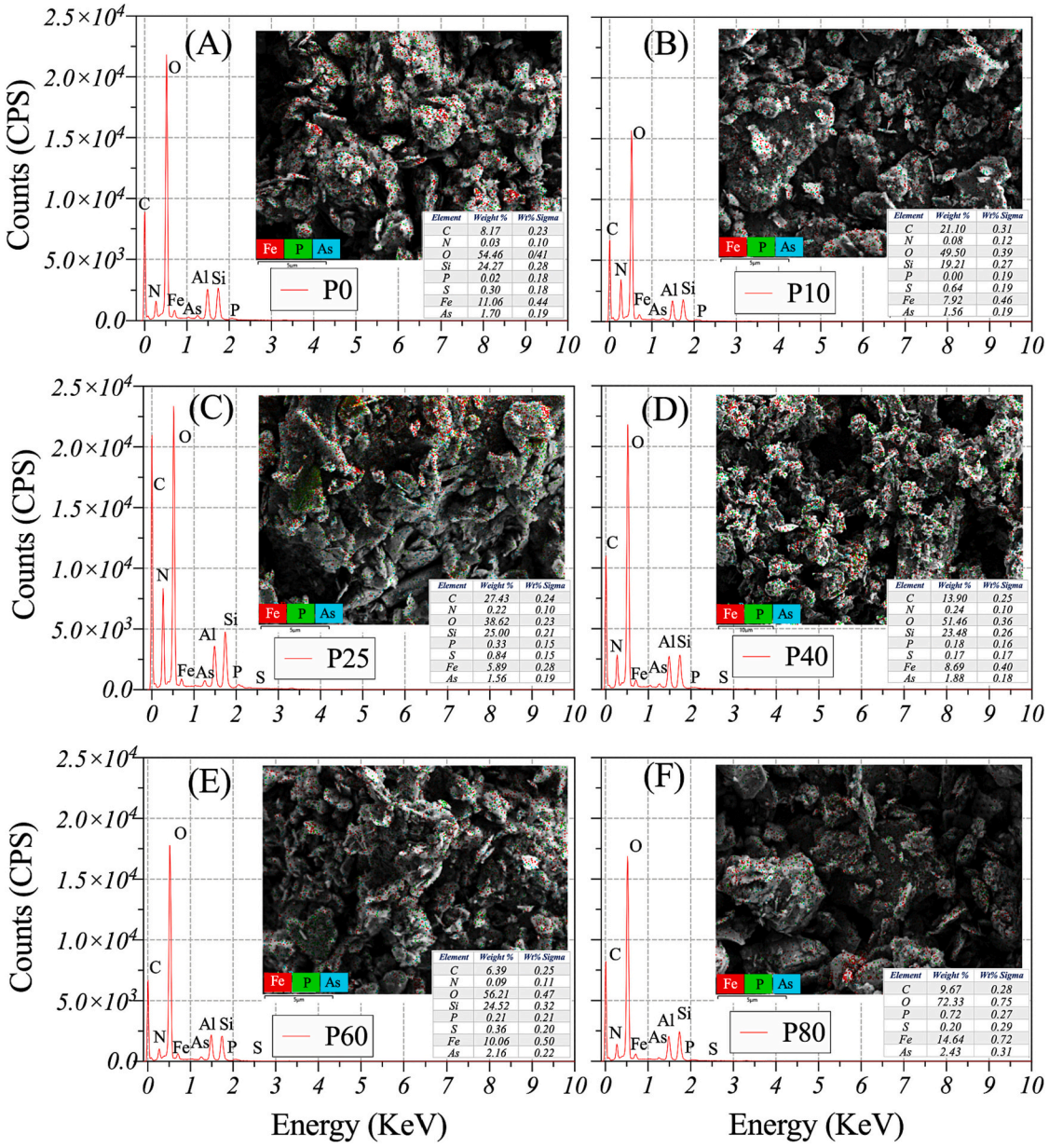

Fig. 7. The energy spectrum and element composition of freeze-dried sediments (60 mg kg^{-1} DW) mapping data after oxalate incubation with the P (KH_2PO_4) addition via detector of energy dispersive analysis X-ray (EDAX). The ultrastructure image of sediments after oxalate incubation with the P addition via scanning transmission electron microscope (STEM) analysis. The red dot represents the Fe distribution in the sediment, the green dot represents the As, and the cyan represents the P; A for the control check (P0); B, C, D, E, and F for 10, 25, 40, 60, and 80 mg L^{-1} P addition treatments, respectively. (For interpretation of the references to color in this figure legend, the reader is referred to the web version of this article.)

mangrove wetlands. Our results outlined concerns on the potential risk of mobilization of arsenic in the mangrove rhizospheric sediments.

CRediT authorship contribution statement

Kang Mei: Conceptualization, Data curation, Formal analysis, Investigation, Methodology, Software, Writing – original draft, Writing – review & editing. **Jingchun Liu:** Writing – review & editing, Funding acquisition, Project administration, Resources, Supervision, Validation. **Liyang Xue:** Visualization, Investigation, Writing – original draft, Writing – review & editing, Formal analysis, Validation. **Jicong Xu:** Writing – original draft, Writing – review & editing. **Wanlin Jiang:** Formal analysis, Investigation. **Zhiwen Tan:** Formal analysis, Investigation. **Anran Li:** Formal analysis, Investigation. **Jinyi Qu:** Formal analysis, Investigation. **Chongling Yan:** Writing – review & editing, Funding acquisition, Project administration, Resources, Supervision, Validation.

Declaration of competing interest

The authors declare that they have no known competing financial interests or personal relationships that could have appeared to influence the work reported in this paper.

Data availability

The authors do not have permission to share data.

Acknowledgements

This study was supported and funded by the major program (31535008) of National Natural Science Foundation of China and National Important Scientific Research Programme of China (2018YFC1406603) and Training Program (S202010384808) of Innovation and Enterpreneurship for Undergraduates, Xiamen University. Thanks to China Scholarship Council (CSC) for providing the support to complete this study during Mr. Kang Mei's academic visit to University of Southern California, United States. The authors are also grateful to the anonymous referees for their constructive comments.

Appendix A. Supplementary data

Supplementary data to this article can be found online at https://doi.org/10.1016/j.marpolbul.2023.114823.

References

Adamson, A., WJJOTES, 1960. In: Physical Chemistry of Surfaces, 124, p. 582.
Amstaetter, K., Borch, T., Larese-Casanova, P., Kappler, A., 2010. Redox transformation of arsenic by Fe(II)-activated goethite (alpha-FeOOH). Environ. Sci. Technol. 44, 102–108.
Biswas, A., Biswas, S., Das, A., Roychowdhury, T., 2018. Spatial variability and competing dynamics of arsenic, selenium, iron and bioavailable phosphate from ground water and soil to paddy plant parts. Groundw. Sustain. Dev. 7, 328–335.
Bose, P., Sharma, A., 2002. Role of iron in controlling speciation and mobilization of arsenic in subsurface environment. Water Res. 36, 4916–4926.
Bowell, R.J.A.G., 1994. In: Sorption of Arsenic by Iron Oxides and Oxyhydroxides in Soils, 9, pp. 279–286.
Burton, E.D., Bush, R.T., Sullivan, L.A., Mitchell, D., 2007. Reductive transformation of iron and sulfur in schwertmannite-rich accumulations associated with acidified coastal lowlands. Geochim. Cosmochim. Acta 71, 4456–4473.
Chancui, Wu., Jie, Liu, Ying, Liang, Yongrong, Jiang, Xuehong, Zhang, 2019. The low molecular weight organic acids in root exudates of Leersia hexandra Swartz and its role in mobilization of insoluble chromium. IOP Conf. Ser. Mater. Sci. Eng. 484, 12009.
Dai, M., Liu, J., Liu, W., Lu, H., Jia, H., Hong, H., Yan, C., 2017. Phosphorus effects on radial oxygen loss, root porosity and iron plaque in two mangrove seedlings under cadmium stress. Mar. Pollut. Bull. 119, 262–269.
Datta, R., Sarkar, D., 2005. Consideration of soil properties in assessment of human health risk from exposure to arsenic-enriched soils. Integr. Environ. Assess. Manag. 1, 55–59.
Elkhatib, E.A., Bennett, O.L., Wright, R.J., 1984. Arsenite sorption and desorption in soils. Soil Sci. Soc. Am. J. 48, 1025–1030.
Esteban, E., Carpena, R.O., Meharg, A.A., 2003. High-affinity phosphate/arsenate transport in white lupin (Lupinus albus) is relatively insensitive to phosphate status. New Phytol 158, 165–173.
Frohne, T., Rinklebe, J., Diaz-Bone, R.A., Du Laing, G., 2011. Controlled variation of redox conditions in a floodplain soil: impact on metal mobilization and biomethylation of arsenic and antimony. Geoderma 160, 414–424.
Gasecka, M., Drzewiecka, K., Magdziak, Z., Piechalak, A., Budka, A., Waliszewska, B., Szentner, K., Golinski, P., Niedzielski, P., Budzynska, S., Mleczek, M., 2021. Arsenic uptake, speciation and physiological response of tree species (Acer pseudoplatanus, Betula pendula and Quercus robur) treated with dimethylarsinic acid. Chemosphere 263, 127859.
Geng, H., Wang, F., Yan, C., Tian, Z., Chen, H., Zhou, B., Yuan, R., Yao, J., 2020. Leaching behavior of metals from iron tailings under varying pH and low-molecular-weight organic acids. J. Hazard. Mater. 383, 121136.
Ghosh, P., Rathinasabapathi, B., Teplitski, M., Ma, L.Q., 2015. Bacterial ability in AsIII oxidation and AsV reduction: relation to arsenic tolerance, P uptake, and siderophore production. Chemosphere 138, 995–1000.
Hasany, S.M., Saeed, M.M., Ahmed, M., 2002. Sorption and thermodynamic behavior of zinc(II)-thiocyanate complexes onto polyurethane foam from acidic solutions. J. Radioanal. Nucl. Chem. 252, 477–484.
Hedley, M.J., Stewart, J.W.B., Chauhan, B.S., 1982. Changes in inorganic and organic soil-phosphorus fractions induced by cultivation practices and by laboratory incubations. Soil Sci. Soc. Am. J. 46, 970–976.
Hu, Y., Li, J.H., Zhu, Y.G., Huang, Y.Z., Hu, H.Q., Christie, P., 2005. Sequestration of as by iron plaque on the roots of three rice (Oryza sativa L.) cultivars in a low-P soil with or without P fertilizer. Environ. Geochem. Health 27, 169–176.
Huang, H., Jia, Y., Sun, G.X., Zhu, Y.G., 2012. Arsenic speciation and volatilization from flooded paddy soils amended with different organic matters. Environ. Sci. Technol. 46, 2163–2168.
Im, J., Yang, K., Moon, S., Kim, Y.J., Nam, K., 2015. Role of phosphate and fe-oxides on the acid-aided extraction efficiency and readsorption of as in field-aged soil. J. Hazard. Mater. 300, 161–166.
Jain, A., Loeppert, R.H., 2000. Effect of competing anions on the adsorption of arsenate and arsenite by ferrihydrite. J. Environ. Qual. 29.
Jain, A., Raven, K.P., Loeppert, R.H., 1999. Arsenite and arsenate adsorption on ferrihydrite: surface charge reduction and net OH- release stoichiometry. Environ Sci Technol 33, 1179–1184.
Ji, Y.P., Luo, W.Q., Lu, G.N., Fan, C., Tao, X.Q., Ye, H., Xie, Y.Y., Shi, Z.Q., Yi, X.Y., Dang, Z., 2019. Effect of phosphate on amorphous iron mineral generation and arsenic behavior in paddy soils. Sci. Total Environ. 657, 644–656.
Jian, L., Junyi, Y., Jingchun, L., Chongling, Y., Haoliang, L., Spencer, K.L., 2017. The effects of sulfur amendments on the geochemistry of sulfur, phosphorus and iron in the mangrove plant (Kandelia obovata (S. L.)) rhizosphere. Mar. Pollut. Bull. 114, 733–741.
Jian, L., Jingchun, L., Chongling, Y., Daolin, D., Haoliang, L., 2019. The alleviation effect of iron on cadmium phytotoxicity in mangrove a. Marina. Alleviation effect of iron on cadmium phytotoxicity in mangrove Avicennia marina (Forsk.) vierh. Chemosphere 226, 413–420.
Jiang, S., Xie, F., Lu, H., Liu, J., Yan, C., 2017. Response of low-molecular-weight organic acids in mangrove root exudates to exposure of polycyclic aromatic hydrocarbons. Environ. Sci. Pollut. Res. Int. 24, 12484–12493.
Jiao, W., Chen, W., Chang, A.C., Page, A.L., 2012. Environmental risks of trace elements associated with long-term phosphate fertilizers applications: a review. Environ. Pollut. 168, 44–53.
Jones, D.L., Dennis, P.G., Owen, A.G., van Hees, P.A.W., 2003. Organic acid behavior in soils - misconceptions and knowledge gaps. Plant Soil 248, 31–41.
Jones, D.L., Shannon, D., Junvee-Fortune, T., Farrar, J.F., 2005. Plant capture of free amino acids is maximized under high soil amino acid concentrations. Soil Biol. Biochem. 37, 179–181.
Kim, E.J., Baek, K., 2015. Enhanced reductive extraction of arsenic from contaminated soils by a combination of dithionite and oxalate. J. Hazard. Mater. 284, 19–26.
Kostka, J.E., Iii, G., 1994. Partitioning and speciation of solid phase iron in saltmarsh sediments. Geochim. Cosmochim. Acta 58, 1701–1710.
La Force, M.J., Hansel, C.M., Fendorf, S.J.E.S., 2000. Arsenic speciation, seasonal transformations, and co-distribution with iron in a mine waste-influenced palustrine emergent wetland. Technology 34, 3937–3943.
Leal-Acosta, M.L., Shumilin, E., Mirlean, N., Sapozhnikov, D., Gordeev, V., 2010. Arsenic and mercury contamination of sediments of geothermal springs, mangrove lagoon and the Santispac Bight, Bahia Concepcion, Baja California Peninsula. Bull. Environ. Contam. Toxicol. 85, 609–613.
LeMonte, J.J., Stuckey, J.W., Sanchez, J.Z., Tappero, R., Rinklebe, J.R., Sparks, D.L., 2017. Sea level rise induced arsenic release from historically contaminated coastal soils. Environ. Sci. Technol. 51, 5913–5922.
Li, R., Chai, M., Li, R., Xu, H., He, B., Qiu, G.Y., 2017a. Influence of introduced Sonneratia apetala on nutrients and heavy metals in intertidal sediments, South China. Environ. Sci. Pollut. Res. Int. 24, 2914–2927.
Li, R.L., Chai, M.W., Li, R.Y., Xu, H.L., He, B., Qiu, G.Y., 2017b. Influence of introduced Sonneratia apetala on nutrients and heavy metals in intertidal sediments, South China. Environ. Sci. Pollut. Res. 24, 2914–2927.
Linquist, B.A., Ruark, M.D., Hill, J.E., 2011. Soil order and management practices control soil phosphorus fractions in managed wetland ecosystems. Nutr. Cycl. Agroecosys. 90, 51–62.
Liu, Y., Shen, L., 2008. From langmuir kinetics to first- and second-order rate equations for adsorption. Langmuir 24, 11625–11630.
Liu, J., Qian, M., Cai, G., Zhu, Q., Ming, H.W., 2007. Variations between rice cultivars in root secretion of organic acids and the relationship with plant cadmium uptake. Environ. Geochem. Health 29, 189–195.
Lu, H., Yan, C., Liu, J., 2007. Low-molecular-weight organic acids exuded by mangrove (Kandelia candel (L.) Druce) roots and their effect on cadmium species change in the rhizosphere. Environ. Exp. Bot. 61, 159–166.
Luo, T., Huang, Z.L., Li, X.Y., Zhang, Y.Y., 2020. Anaerobic microbe mediated arsenic reduction and redistribution in coastal wetland soil. Sci. Total Environ. 727, 8.
Magdziak, Z., Gasecka, M., Budka, A., Golinski, P., Mleczek, M., 2020. Profile and concentration of the low molecular weight organic acids and phenolic compounds created by two-year-old Acer platanoides seedlings growing under different as forms. J. Hazard. Mater. 392, 122280.
Manceau, A., Boisset, M.-C., Sarret, G., Hazemann, J.-L., Mench, M., Cambier, P., Prost, R.J.E.S., 1996. Direct determination of lead speciation in contaminated soils by EXAFS spectroscopy. Technology 30, 1540–1552.
Mandal, B.K., Suzuki, K.T., 2002. Arsenic round the world: a review. Talanta 58, 201–235.
Mandal, S.K., Ray, R., González, A., Pokrovsky, O.S., Kumar, T., 2019. Accumulation, transport and toxicity of arsenic in the Sundarbans mangrove, India. Geoderma 354, 113891.
Manning, B.A., Fendorf, S.E., Goldberg, S., 1998. Surface structures and stability of arsenic(III) on goethite: spectroscopic evidence for inner-sphere complexes. Environ Sci Technol 32, 2383–2388.
Mei, K., Liu, J., Shi, R., Guo, X., Lu, H., Yan, C., 2020. The migrated behavior and bioavailability of arsenic in mangrove sediments affected by pH and organic acids. Mar. Pollut. Bull. 159, 111480.
Mei, K., Liu, J., Fan, J., Guo, X., Wu, J., Zhou, Y., Lu, H., Yan, C., 2021. Low-level arsenite boosts rhizospheric exudation of low-molecular-weight organic acids from mangrove seedlings (Avicennia marina): arsenic phytoextraction, removal, and detoxification. Sci. Total Environ. 775, 145685.
Mei, K., Wu, G., Liu, J., Jiajia, W., Hong, H., Lu, H., Yan, C., 2022. Dynamics of low-molecular-weight organic acids for the extraction and sequestration of arsenic species and heavy metals using mangrove sediments. Chemosphere 286, 131820.
Mirlean, N., Medeanic, S., Garcia, F.A., Travassos, M.P., Baisch, P., 2012. Arsenic enrichment in shelf and coastal sediment of the brazilian subtropics. Cont. Shelf Res. 35, 129–136.

Mohan, D., Pittman Jr., C.U., 2007. Arsenic removal from water/wastewater using Adsorbents—A critical review. J. Hazard. Mater. 142 (1-2), 1–53.
Mohapatra, D., Singh, P., Zhang, W., Pullammanappallil, P., 2005. The effect of citrate, oxalate, acetate, silicate and phosphate on stability of synthetic arsenic-loaded ferrihydrite and Al-ferrihydrite. J. Hazard. Mater. 124, 95–100.
Nguyen, Thanh-Nho, Cyril, Marchand, Emilie, Strady, Huu-Phat, Tran-Thi, Nhu-Trang, 2019. Bioaccumulation of some trace elements in tropical mangrove plants and snails (Can Gio, Vietnam). Environ. Pollut. 248, 635–645.
Onireti, O.O., Lin, C., 2016. Mobilization of soil-borne arsenic by three common organic acids: dosage and time effects. Chemosphere 147, 352–360.
Pan, F., Liu, H., Guo, Z., Cai, Y., Fu, Y., Wu, J., Wang, B., Gao, A., 2019. Metal/metalloid and phosphorus characteristics in porewater associated with manganese geochemistry: a case study in the Jiulong River estuaryChina. Environ Pollut 255, 113134.
Rozan, T.F., Taillefert, M., Trouwborst, R.E., Glazer, B.T., Ma, S., Herszage, J., Valdes, L. M., Iii, P., 2002. Iron-sulfurphosphorus cycling in the sediments of a shallow coastal bay: implications for sediment nutrient release and benthic macroalgal blooms. Limnol. Oceanogr. 47 (5), 1346–1354.
Shaheen, S.M., Rinklebe, J., Frohne, T., White, J.R., DeLaune, R.D., 2016. Redox effects on release kinetics of arsenic, cadmium, cobalt, and vanadium in wax Lake deltaic freshwater marsh soils. Chemosphere 150, 740–748.
Strobel, B.W., 2001. Influence of vegetation on low-molecular-weight carboxylic acids in soil solution—a review. Geoderma 99, 169–198.
Stumm, W., 1992. Chemistry of the Solid-water Interface: Processes at the Mineral-water and Particle-water Interface in Natural Systems. John Wiley & Son Inc., New York.
Sun, Q., Sheng, Y., Yang, J., Di Bonito, M., Mortimer, R.J.G., 2016. Dynamic characteristics of sulfur, iron and phosphorus in coastal polluted sediments, North China. Environ. Pollut. 219, 588–595.
Sun, Q., Ding, S., Zhang, L., Chen, M., Zhang, C., 2017. A millimeter-scale observation of the competitive effect of phosphate on promotion of arsenic mobilization in sediments. Chemosphere 180, 285–294.
Vitkova, M., Komarek, M., Tejnecky, V., Sillerova, H., 2015. Interactions of nano-oxides with low-molecular-weight organic acids in a contaminated soil. J. Hazard. Mater. 293, 7–14.
Wang, W., Wang, W.X., 2017. Trace metal behavior in sediments of Jiulong River estuary and implication for benthic exchange fluxes. Environ. Pollut. 225, 598–609.
Weber, T.W., Chakravorti, R.K.J.A.J., 1974. In: Pore and Solid Diffusion Models for Fixed-bed Adsorbers, 20, pp. 228–238.
Wu, L., Liu, C., Hu, Y., Tan, B., He, Y., Li, N., 2020. Dephosphorization using ceramsites modified by coprecipitation with FeSo4 and KMnO4 and high-temperature combustion. J. Water Process Eng. 34, 101162.
Xiang, L., Chen, X.-T., Yu, P.-F., Li, X.-H., Zhao, H.-M., Feng, N.-X., Li, Y.-W., Li, H., Cai, Q.-Y., Mo, C.-H., 2020. Oxalic acid in root exudates enhances accumulation of perfluorooctanoic acid in lettuce. Environ. Sci. Technol. 54, 13046–13055.
Xu, L., Wu, X., Wang, S., Yuan, Z., Xiao, F., Yang, M., Jia, Y., 2016. Speciation change and redistribution of arsenic in soil under anaerobic microbial activities. J. Hazard. Mater. 301, 538–546.
Zhang, Peng, Yao, Weiyu, Yuan, Songhu, 2017. Citrate-enhanced release of arsenic during pyrite oxidation at circumneutral conditions. Water Res. 109, 245–252.